Space Weather

RESEARCH ARTICLE
10.1029/2023SW003824

# Prediction of the SYM-H Index Using a Bayesian Deep Learning Method With Uncertainty Quantification

**Yasser Abduallah[1,2], Khalid A. Alobaid[1,2,3], Jason T. L. Wang[1,2], Haimin Wang[1,4,5], Vania K. Jordanova[6], Vasyl Yurchyshyn[5], Huseyin Cavus[7,8], and Ju Jing[1,4,5]**

[1]Institute for Space Weather Sciences, New Jersey Institute of Technology, Newark, NJ, USA, [2]Department of Computer Science, New Jersey Institute of Technology, Newark, NJ, USA, [3]College of Applied Computer Sciences, King Saud University, Riyadh, Saudi Arabia, [4]Center for Solar-Terrestrial Research, New Jersey Institute of Technology, Newark, NJ, USA, [5]Big Bear Solar Observatory, New Jersey Institute of Technology, Big Bear City, CA, USA, [6]Los Alamos National Laboratory, Space Science and Applications, Los Alamos, NM, USA, [7]Department of Physics, Canakkale Onsekiz Mart University, Canakkale, Turkey, [8]Harvard-Smithsonian Center for Astrophysics, Cambridge, MA, USA

**Abstract** We propose a novel deep learning framework, named SYMHnet, which employs a graph neural network and a bidirectional long short-term memory network to cooperatively learn patterns from solar wind and interplanetary magnetic field parameters for short-term forecasts of the SYM-H index based on 1- and 5-min resolution data. SYMHnet takes, as input, the time series of the parameters' values provided by NASA's Space Science Data Coordinated Archive and predicts, as output, the SYM-H index value at time point $t + w$ hours for a given time point $t$ where $w$ is 1 or 2. By incorporating Bayesian inference into the learning framework, SYMHnet can quantify both aleatoric (data) uncertainty and epistemic (model) uncertainty when predicting future SYM-H indices. Experimental results show that SYMHnet works well at quiet time and storm time, for both 1- and 5-min resolution data. The results also show that SYMHnet generally performs better than related machine learning methods. For example, SYMHnet achieves a forecast skill score (FSS) of 0.343 compared to the FSS of 0.074 of a recent gradient boosting machine (GBM) method when predicting SYM-H indices (1 hr in advance) in a large storm (SYM-H = −393 nT) using 5-min resolution data. When predicting the SYM-H indices (2 hr in advance) in the large storm, SYMHnet achieves an FSS of 0.553 compared to the FSS of 0.087 of the GBM method. In addition, SYMHnet can provide results for both data and model uncertainty quantification, whereas the related methods cannot.

**Plain Language Summary** In the past several years, machine learning and its subfield, deep learning, have attracted considerable interest. Computer vision, natural language processing, and social network analysis make extensive use of machine learning algorithms. Recent applications of these algorithms include the prediction of solar flares and the forecasting of geomagnetic indices. In this paper, we propose an innovative machine learning method that utilizes a graph neural network and a bidirectional long short-term memory network to cooperatively learn patterns from solar wind and interplanetary magnetic field parameters to provide short-term predictions of the SYM-H index. In addition, we present techniques for quantifying both data and model uncertainties in the output of the proposed method.

**Key Points:**

- SYMHnet is a novel deep learning method for making short-term predictions of the SYM-H index (1 or 2 hr in advance)
- With Bayesian inference, SYMHnet can quantify both aleatoric (data) and epistemic (model) uncertainties in making its prediction
- SYMHnet generally performs better than related machine learning methods for SYM-H forecasting

**Correspondence to:**
J. T. L. Wang,
wangj@njit.edu

**Citation:**
Abduallah, Y., Alobaid, K. A., Wang, J. T. L., Wang, H., Jordanova, V. K., Yurchyshyn, V., et al. (2024). Prediction of the SYM-H index using a Bayesian deep learning method with uncertainty quantification. *Space Weather*, *22*, e2023SW003824. https://doi.org/10.1029/2023SW003824

Received 6 DEC 2023
Accepted 26 JAN 2024

**Author Contribution:**
**Data curation:** Yasser Abduallah
**Formal analysis:** Yasser Abduallah
**Investigation:** Yasser Abduallah
**Methodology:** Yasser Abduallah
**Resources:** Yasser Abduallah
**Software:** Yasser Abduallah
**Validation:** Yasser Abduallah
**Visualization:** Yasser Abduallah
**Writing – original draft:** Yasser Abduallah
**Writing – review & editing:** Yasser Abduallah



## 1. Introduction

Geomagnetic activities and events are known to have a substantial impact on the Earth. They can damage and affect technological systems such as telecommunication networks, power transmission systems, and spacecraft (Jordanova et al., 2020; Ayala Solares et al., 2016). These activities are massive and scale on orders of magnitude (Newell et al., 2007). It may take a few days to recover from the damage, depending on its severity. These activities and events cannot be ignored regardless of whether they are in regions at high, medium, or low latitudes (Carter et al., 2016; Gaunt & Coetzee, 2007; Moldwin & Tsu, 2016; Tozzi et al., 2019; Viljanen et al., 2014). Therefore, several activity indices have been developed to measure the intensity of the geomagnetic effects. These indices characterize the magnitude of the disturbance over time. Modeling and forecasting these geomagnetic indices have become a crucial area of study in space weather research.

Some indices, such as Kp, describe the overall level of geomagnetic activity while others, such as the disturbance storm time (Dst) index (Woodroffe et al., 2016), describe a specific area of geomagnetic activity. The Dst index has been used to classify a storm based on its intensity (Bala & Reiff, 2012; Gruet et al., 2018; Lazzús et al., 2017;

Lu et al., 2016; Xu et al., 2023). The storm is intense when Dst is less than −100 nT, moderate when Dst is between −100 and −50 nT, and weak when Dst is greater than −50 nT (Gruet et al., 2018; Nuraeni et al., 2022). Another important index is the symmetric H-component index (SYM-H), which is used to represent the longitudinally symmetric disturbance of the intensity of the ring current during geomagnetic storms. The SYM-H index is the 1-min version of the DST index, obtained by data from more stations (Rangarajan, 1989; Siciliano et al., 2021; Vichare et al., 2019; Wanliss & Showalter, 2006). On the other hand, ASY-H (the asymmetric geomagnetic disturbance of the horizontal component) is quantified as the longitudinally asymmetric part of the geomagnetic disturbance field at low latitude to midlatitude. In addition, there are other indices that can be used to measure the activity of the storm as described in Mayaud (1980).

A lot of efforts have been devoted to developing strategies to alleviate the geomagnetic effects on technologies and humans, but it is almost impossible to offer complete protection from the effects (Siciliano et al., 2021). Some of these strategies are to predict the occurrence and intensity of geomagnetic storms to offer some level of mitigation of their damaging effects. For example, Burton et al. (1975) established an empirical connection between interplanetary circumstances and Dst using a linear forecasting model. Temerin and Li (2002) developed an explicit model to predict Dst on the basis of solar wind data for the years 1995–1999, by finding functions and values of free parameters that minimize the root square error (RMS error) between their model and the measured Dst. Wang et al. (2003) used differential equation models to examine the effect of the dynamic pressure of the solar wind on the decay and injection of the ring current. Yurchyshyn et al. (2004) proposed that the hourly averaged magnitude of the $Bz$ component of the magnetic field in interplanetary ejecta is correlated with the speed of the CME, which may open a way to predict the Dst index using CME parameters. Ayala Solares et al. (2016) performed predictions of global magnetic disturbance in near-Earth space in a case study for the Kp index using Nonlinear AutoRegressive with eXogenous (NARX) models. Due to the intrinsic complex response of the circumterrestrial environment to changes in the interplanetary medium, these simple models were unable to properly and fully depict the evolution of the solar wind-magnetosphere-ionosphere system (Consolini & Chang, 2001; Klimas et al., 1996; Siciliano et al., 2021). To surpass the limitations of simple models and acquire the complex response of the magnetosphere, researchers resorted to more advanced models such as artificial neural networks (ANNs).

The use of ANNs focused on the prediction of the Dst and Kp indices. Gleisner et al. (1996) constructed the first Dst prediction model employing a time-delay ANN with solar wind parameters as input variables. Lazzús et al. (2017) created a particle swarm optimization method to train ANN connection weights to improve the accuracy of the prediction of the Dst index. Bala and Reiff (2012) combined ANNs and physical models with solar wind and interplanetary magnetic field parameters such as velocity, interplanetary magnetic field (IMF) magnitude, and clock angle. Chandorkar et al. (2017) used Gaussian processes (GP) to build an autoregressive model to predict the Dst index 1 hr in advance based on the past solar wind velocity, the IMF component $B_z$, and the values of the Dst index. This method generated a predictive distribution rather than a single prediction point. However, the mean values of the estimations are not as accurate as those generated by ANNs. Gruet et al. (2018) overcame the poor performance of GP and constructed a Dst index estimation model by merging GP with a long short-term memory (LSTM) network to obtain more accurate results. More recently, Xu et al. (2023) developed a new GP regression model that performed better than related distance correlation learning methods (Lu et al., 2016) in forecasting the Dst index during intense geomagnetic storms. Rastätter et al. (2013) compared the effectiveness of 30 Dst forecast models and found that none of the models performed consistently the best for all events.

Relatively few researchers have focused on the prediction of SYM-H. This happens probably because of the high temporal resolution of 1 min for the SYM-H index, which gives rise to a more difficult problem in estimating SYM-H due to its highly oscillating nature (Siciliano et al., 2021). However, some SYM-H index prediction techniques have been reported in the literature. Cai et al. (2010) presented the first 5-min average estimates of the SYM-H index throughout large storms between 1998 and 2006 using a NARX neural network with IMF and solar wind data. Bhaskar and Vichare (2019) predicted both the SYM-H and ASY-H indices for solar cycle 24 by employing the NARX neural network in a similar way. Both Bhaskar and Vichare (2019) and Cai et al. (2010) used the IMF magnitude ($B$), $B_y$, and $B_z$ components, as well as the density and velocity of the solar wind as input data for their models. Siciliano et al. (2021) provided a comprehensive examination of two well-known deep learning models, namely long short-term memory (LSTM) and a convolutional neural network (CNN), with an average temporal resolution of 5 min for the estimation of SYM-H index values (1 hr in advance). The authors used the IMF component $B_z$, squared values of the magnitude of the IMF $B$ and the $B_y$ component, measured at L1 by the ACE satellite in GSM coordinates. Collado-Villaverde et al. (2021) created neural network models for the

**Table 1**
*Storms Used to Train SYMHnet*

| Storm # | Start date | End date | Min SYM-H (nT) | Max SYM-H (nT) |
|---|---|---|---|---|
| 1 | 02/14/1998 | 02/22/1998 | −119 | 12 |
| 2 | 08/02/1998 | 08/08/1998 | −168 | 25 |
| 3 | 09/19/1998 | 09/29/1998 | −213 | 8 |
| 4 | 02/16/1999 | 02/24/1999 | −127 | 28 |
| 5 | 10/15/1999 | 10/25/1999 | −218 | 42 |
| 6 | 07/09/2000 | 07/19/2000 | −335 | 76 |
| 7 | 08/06/2000 | 08/16/2000 | −235 | 10 |
| 8 | 09/15/2000 | 09/25/2000 | −196 | 43 |
| 9 | 11/01/2000 | 11/15/2000 | −174 | 43 |
| 10 | 03/14/2001 | 03/24/2001 | −165 | 22 |
| 11 | 04/06/2001 | 04/16/2001 | −275 | 32 |
| 12 | 10/17/2001 | 10/22/2001 | −210 | 37 |
| 13 | 10/31/2001 | 11/10/2001 | −313 | 43 |
| 14 | 05/17/2002 | 05/27/2002 | −113 | 101 |
| 15 | 11/15/2003 | 11/25/2003 | −488 | 10 |
| 16 | 07/20/2004 | 07/30/2004 | −208 | 32 |
| 17 | 05/10/2005 | 05/20/2005 | −302 | 64 |
| 18 | 04/09/2006 | 04/19/2006 | −110 | 24 |
| 19 | 10/09/2006 | 12/19/2006 | −206 | 39 |
| 20 | 03/01/2012 | 03/11/2012 | −149 | 49 |

**Table 2**
*Storms Used to Validate SYMHnet*

| Storm # | Start date | End date | Min SYM-H (nT) | Max SYM-H (nT) |
|---|---|---|---|---|
| 21 | 04/28/1998 | 05/08/1998 | −268 | 50 |
| 22 | 09/19/1999 | 09/26/1999 | −160 | 64 |
| 23 | 10/25/2003 | 11/03/2003 | −427 | 33 |
| 24 | 06/18/2015 | 06/28/2015 | −207 | 77 |
| 25 | 09/01/2017 | 09/11/2017 | −144 | 54 |

SYM-H and ASY-H predictions by combining CNN and LSTM. The authors considered 42 geomagnetic storms between 1998 and 2018 for model training, validation, and testing purposes. Iong et al. (2022) developed a model using gradient boosting machines to predict the SYM-H index (1 and 2 hr in advance) with a temporal resolution of 5 min.

In this paper, we present a new method, named SYMHnet, that utilizes cooperative learning of a graph neural network (GNN) and a bidirectional long short-term memory (BiLSTM) network with Bayesian inference to conduct short-term (1 or 2 hr in advance) predictions of the SYM-H index for solar cycles 23 and 24. We consider temporal resolutions of 1 and 5 min, respectively, for the SYM-H index. To our knowledge, this is the first time that 1-min resolution data have been used to predict the SYM-H index. Furthermore, our method can quantify both model and data uncertainties when producing prediction results, whereas related machine learning methods cannot.

The remainder of this paper is organized as follows. Section 2 describes the data, including the solar wind and IMF parameters, as well as geomagnetic storms, used in this study. Section 3 presents the methodology, explaining the SYMHnet framework, its architecture, and the uncertainty quantification algorithm. Section 4 evaluates the performance of SYMHnet on 1- and 5-min resolution data. We also report the experimental results obtained by comparing SYMHnet with related machine learning methods on 5-min resolution data. Section 5 presents a discussion and concludes the paper.

## 2. Database

In training and evaluating SYMHnet, we built a database that combines the solar wind and IMF parameters with the geomagnetic storms studied in this paper. This database contains 42 storms selected from the past two solar cycles (#23 and #24). The storms occurred between 1998 and 2018.

### 2.1. Solar Wind and IMF Parameters

We consider seven solar wind, IMF, and derived parameters: IMF magnitude ($B$), $B_y$, and $B_z$ components, flow speed, proton density, electric field and flow pressure. These parameters have been used in related studies (Bhaskar & Vichare, 2019; Cai et al., 2010; Denton et al., 2016; Iong et al., 2022). The parameters' values along with the SYM-H index values are collected from the NASA Space Science Data Coordinated Archive available at https://nssdc.gsfc.nasa.gov (King & Papitashvili, 2005). Data are collected with 1- and 5-min resolutions.

### 2.2. Geomagnetic Storms

We work with the same storms as those considered in previous studies (Collado-Villaverde et al., 2021; Iong et al., 2022; Siciliano et al., 2021). Table 1 lists the storms used to train SYMHnet. Table 2 lists the storms used to validate SYMHnet. Table 3 lists the storms used to test SYMHnet. The training set, validation set, and test set are disjoint. Thus, SYMHnet can make predictions on storms that it has never seen during training. Note that each storm period listed in Tables 1–3 contains both quiet time and storm time, as indicated by the maximum SYM-H and minimum SYM-H values in the period.

## 3. Methodology

Machine learning (ML) and its subfield, deep learning (DL) (Goodfellow et al., 2016), have been used extensively in the space weather community for predicting solar flares (Abduallah et al., 2021; Huang et al., 2018; Liu et al., 2019), flare precursors (Chen et al., 2019), coronal mass ejections

**Table 3**
*Storms Used to Test SYMHnet*

| Storm # | Start date | End date | Min SYM-H (nT) | Max SYM-H (nT) |
|---|---|---|---|---|
| 26 | 06/22/1998 | 06/30/1998 | −120 | 39 |
| 27 | 11/02/1998 | 11/12/1998 | −179 | 19 |
| 28 | 01/09/1999 | 01/18/1999 | −111 | 9 |
| 29 | 04/13/1999 | 04/19/1999 | −122 | 63 |
| 30 | 01/16/2000 | 01/26/2000 | −101 | 21 |
| 31 | 04/02/2000 | 04/12/2000 | −315 | 16 |
| 32 | 05/19/2000 | 05/28/2000 | −159 | 47 |
| 33 | 03/26/2001 | 04/04/2001 | −434 | 109 |
| 34 | 05/26/2003 | 06/06/2003 | −162 | 10 |
| 35 | 07/08/2003 | 07/18/2003 | −125 | 23 |
| 36 | 01/18/2004 | 01/27/2004 | −137 | 41 |
| 37 | 11/04/2004 | 11/14/2004 | −393 | 92 |
| 38 | 09/10/2012 | 10/05/2012 | −138 | 18 |
| 39 | 05/28/2013 | 06/04/2013 | −134 | 37 |
| 40 | 06/26/2013 | 07/04/2013 | −110 | 19 |
| 41 | 03/11/2015 | 03/21/2015 | −233 | 62 |
| 42 | 08/22/2018 | 09/03/2018 | −205 | 26 |

(Alobaid et al., 2022; Liu et al., 2020), solar energetic particles (Abduallah et al., 2022; Laurenza et al., 2009; Lavasa et al., 2021; Núñez, 2011; Stumpo et al., 2021), and geomagnetic indices (Amata et al., 2008; Bala & Reiff, 2012; Bhaskar & Vichare, 2019; Collado-Villaverde et al., 2021; Gruet et al., 2018; Lazzús et al., 2017; Pallocchia et al., 2006; Siciliano et al., 2021). Different from the existing methods, SYMHnet combines a graph neural network (GNN) and a bidirectional long short-term memory (BiLSTM) network to jointly learn patterns from input data. GNN learns the relationships among the parameter values in the input data, while BiLSTM captures the temporal dynamics of the input data. As our experimental results show later, this combined learning framework works well and generally performs better than related machine learning methods for SYM-H index forecasting.

### 3.1. Parameter Graph

We construct an undirected unweighted fully connected graph (FCG) for the solar wind, the IMF and the derived parameters considered in this study, where each node represents a parameter and there is an edge between every two nodes. Because the parameter values are time series, we obtain a time series of parameter graphs where the topologies of the graphs are the same, but the node values vary as time goes on. For example, Figure 1 shows three parameter graphs constructed at time points $t$, $t + 1$, $t + 2$, respectively, with a resolution of 1 min to predict the SYM-H index 1 hr in advance. In Figure 1, the leftmost graph at $t$ contains the values of the seven parameters, represented by seven nodes or circles, at the time point $t$. The FCG symbol in the center indicates that this is a fully connected graph in which every two nodes are connected by an edge. (For simplicity, only a portion of the edges are shown in the figure). Furthermore, the graph contains a node that represents the value of the SYM-H index at the time point $t + 1$ hr. During training, this SYM-H index value is used as the label for the graph. The GNN in SYMHnet will learn the relationships among the parameters' values and the relationships between the parameters' values and the label. If we want to predict the SYM-H index 2 hr in advance, then the label will be the SYM-H index value at the time point $t + 2$ hr.

The middle graph at $t + 1$ in Figure 1 contains the values of the seven parameters at the time point $t + 1$ min. In addition, this graph contains the SYM-H index value at the time point ($t + 1$ min) + 1 hr, which is the label for this

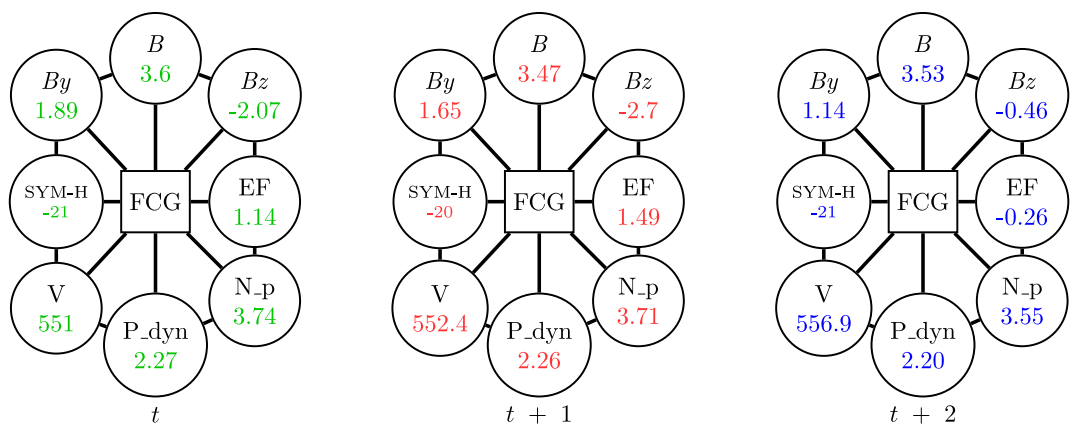


**Figure 1.** Illustration of the parameter graphs constructed at time points $t$, $t + 1$, $t + 2$, respectively with a resolution of 1 min for predicting the SYM-H index 1 hr in advance. Each graph contains seven parameters: IMF magnitude ($B$), $B_y$ component, $B_z$ component, electric field (EF), proton density (N_p), flow pressure (P_dyn), and flow speed (V). The colored values in the graphs represent the parameters' values that change as time goes on, while the topologies of the graphs remain the same. The value in the SYM-H node in a graph is the label of the graph. The FCG symbol in a graph indicates that the graph is fully connected.

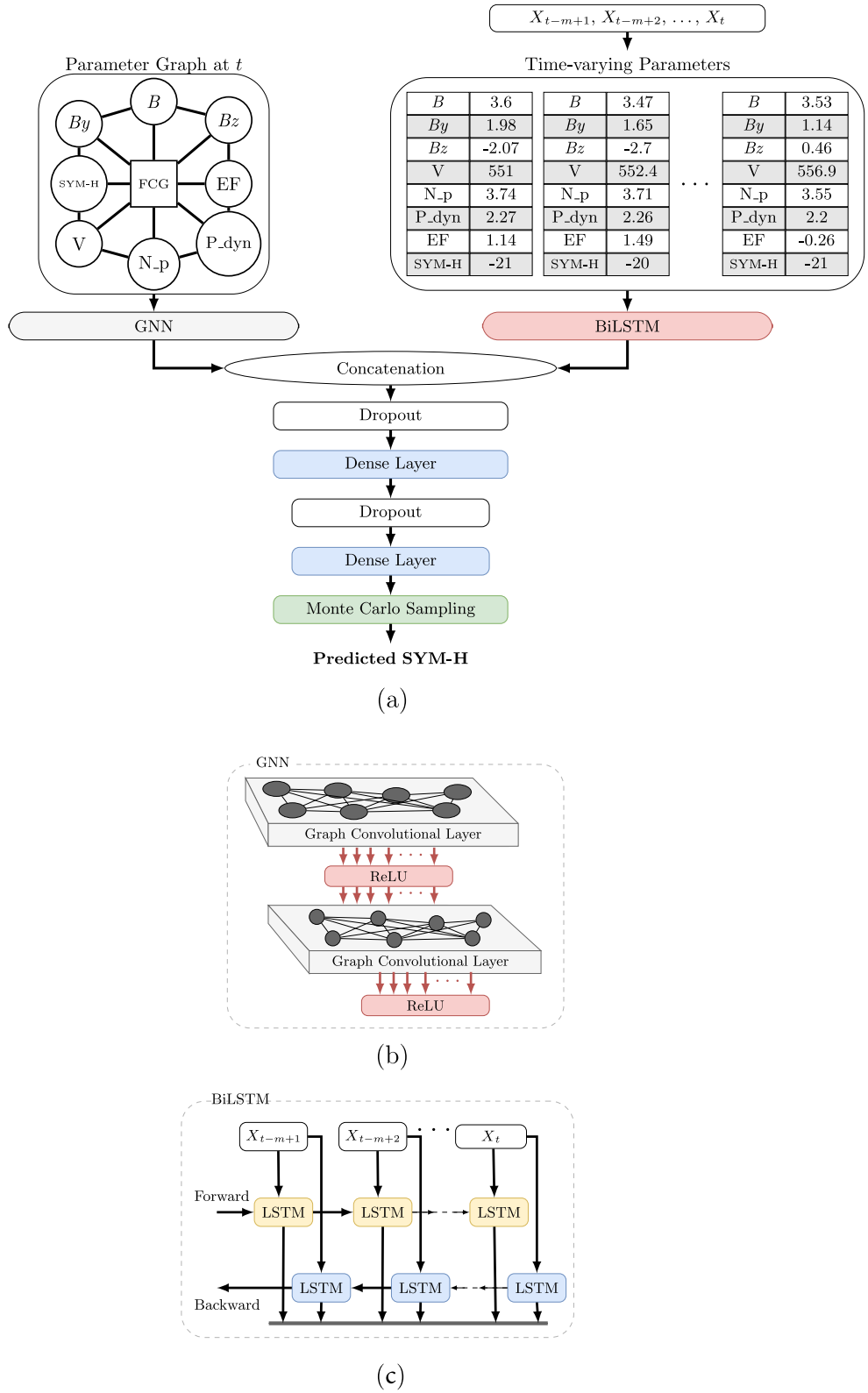


**Figure 2.** The SYMHnet framework: (a) the overall architecture of SYMHnet, (b) the architecture of its GNN component, and (c) the architecture of its BiLSTM component. The input parameter graph is for illustration; the actual graph in the implementation is a fully connected graph (FCG). $B$ = IMF magnitude (B), $By$ = $By$ component, $Bz$ = $Bz$ component, EF = Electric field, N_p = Proton density, P_dyn = Flow pressure, and V = Flow speed.

**Table 4**
*Architecture Details of SYMHnet*

| Component | Parameter | Value |
|---|---|---|
| Forward LSTM | Number of LSTM units | 400 |
| Backward LSTM | Number of LSTM units | 400 |
| | Activation function | ReLU |
| GNN | Number of nodes | 8 |
| | Number of edges | 56 |
| | Activation function | ReLU |
| | Number of graph convolutional layers | 2 |
| Dense layer | Number of neurons | 200 |

graph. If we want to predict the SYM-H index 2 hr in advance, then the label will be the SYM-H index value at the time point ($t$ + 1 min) + 2 hr.

The rightmost graph at $t$ + 2 in Figure 1 contains the values of the seven parameters at the time point $t$ + 2 min. Additionally, this graph contains the SYM-H index value at the time point ($t$ + 2 min) + 1 hr, which is the label for this graph. If we want to predict the SYM-H index 2 hr in advance, then the label will be the SYM-H index value at the time point ($t$ + 2 min) + 2 hr.

During testing/prediction, given the values of the seven parameters at a time point $t'$ (without a label), SYMHnet will predict the label, which is the SYM-H index value at the time point $t'$ + 1 hr (for 1-hr ahead predictions) or the SYM-H index value at the time point $t'$ + 2 hr (for 2-hr ahead predictions), as detailed in Section 3.2.

### 3.2. The SYMHnet Framework

Figure 2 illustrates the SYMHnet framework. During training, we feed the input data sample at each time point in turn to SYMHnet. The input data sample at the time point $t$ consists of the parameter graph $G_t$ constructed at $t$ and a sequence of $m$ records $X_{t-m+1}, X_{t-m+2}, \ldots, X_t$ where $X_i$, $t - m + 1 \leq i \leq t$, represents the record collected at the time point $i$. $X_i$ contains the seven values of the solar wind and IMF parameters along with the SYM-H index value at the time point $i$. Including previous SYM-H index values in the input to predict future SYM-H indices improves prediction accuracy (Iong et al., 2022). The number of records, $m$, in the input is set to 10 which was determined by our experiments. When $m < 10$, BiLSTM cannot effectively capture the temporal patterns in the data. When $m > 10$, it causes additional overhead for larger sequence sizes without improving prediction accuracy. The label of the graph $G_t$ is used as the label of the input data sample at the time point $t$.

The parameter graph $G_t$ is sent to SYMHnet's GNN component (Panagopoulos et al., 2021) while the sequence of $m$ records, $X_{t-m+1}, X_{t-m+2}, \ldots, X_t$, is sent to SYMHnet's BiLSTM component (Abduallah et al., 2022). The GNN, illustrated in Figure 2b, contains a graph convolutional layer followed by a rectified linear unit (ReLU), which is followed by another graph convolutional layer and ReLU. The BiLSTM network, illustrated in Figure 2c, is composed of two LSTM layers (Hochreiter & Schmidhuber, 1997) with opposite directions when processing the data. This architecture allows the BiLSTM network to use one LSTM layer to read the sequence from the end to the beginning, denoted as forward, and the other LSTM layer to read the sequence from the beginning to the end, denoted as backward. GNN is good for learning the correlations between nodes (parameters) in a graph (Panagopoulos et al., 2021) while BiLSTM is suitable for learning the temporal patterns in time series (Abduallah et al., 2022; Siami-Namini et al., 2019). SYMHnet combines the learned parameter correlations and temporal patterns into a joint pattern, which is then passed to two dropout and dense layers.

A dropout layer provides a mechanism to randomly drop a percentage of neurons to avoid over-fitting on the training data so that the SYMHnet model can generalize to unseen test data. It also enables the Monte Carlo (MC) sampling method described in Section 3.3 because the internal structure of the network is slightly different each time neurons are dropped (Gal & Ghahramani, 2016; Jiang et al., 2021). Each neuron in a dense layer connects to every neuron in the preceding layer (Goodfellow et al., 2016). The dense layer helps to change the dimensionality of the output of the preceding layer so that the SYMHnet model can easily define the relationship between the values of the data on which the model works. In this way, we better train our model, and the model learns things more effectively. Table 4 summarizes the details of the model architecture.

**Table 5**
*Hyperparameter Values Used by SYMHnet*

| Parameter | Value |
|---|---|
| Dropout rate | 0.5 |
| Batch size | 1,024 |
| Epochs | 50 |
| Optimizer | RMSProp |
| Learning rate | 0.0002 |
| Loss function | MSE |

During testing/prediction, we feed an unlabeled test data sample to SYMHnet where the test data sample is the same as the training data sample, except that the test data sample does not have a label. The trained SYMHnet model will predict the label based on the input test data sample. SYMHnet uses the MC dropout sampling method described in Section 3.3 to produce, for a test data sample, a predicted SYM-H index value accompanied by results of aleatoric uncertainty and epistemic uncertainty.

**Table 6**
*Results of the Ablation Study Based on 1-Min Resolution Data*

| Metric | Hour-ahead | SYMHnet | SYMHnet-B | SYMHnet-G | SYMHnet-BG |
|---|---|---|---|---|---|
| RMSE | 1 | **3.002** (2.169) | 3.210 (2.319) | 4.194 (3.030) | 5.348 (2.957) |
| | 2 | **3.171** (2.201) | 3.432 (2.382) | 4.369 (3.033) | 5.623 (3.066) |
| FSS | 1 | **0.668** (0.131) | 0.563 (0.003) | 0.007 (0.012) | −0.644 (0.015) |
| | 2 | **0.760** (0.089) | 0.387 (0.031) | −0.367 (0.016) | −0.731 (0.031) |
| $R^2$ | 1 | **0.993** (0.003) | 0.913 (0.001) | 0.789 (0.001) | 0.602 (0.001) |
| | 2 | **0.993** (0.003) | 0.908 (0.002) | 0.776 (0.002) | 0.594 (0.002) |

### 3.3. Uncertainty Quantification

Quantification of uncertainty is essential for the reproducibility and validation of a model (Volodina & Challenor, 2021). Uncertainty quantification with deep learning has been used in computer vision (Kendall & Gal, 2017), space weather (Gruet et al., 2018), and solar physics (Jiang et al., 2021). There are two types of uncertainty: aleatoric and epistemic. Aleatoric uncertainty captures the inherent randomness of data, hence also referred to as data uncertainty. Epistemic uncertainty occurs due to the inexact weight calculations in a neural network and is also known as model uncertainty.

In incorporating Bayesian inference into SYMHnet, our goal is to find the posterior distribution over the weights of the network, $W$, given the observed training data, $X$, and the labels $Y$, that is, $P(W|X, Y)$. The posterior distribution is intractable (Jiang et al., 2021), and one has to approximate the weight distribution (Denker & LeCun, 1990). We use variational inference as suggested by Graves (2011) to learn the variational distribution on the weights of the network, $q(W)$, by minimizing the Kullback–Leibler (KL) divergence of $q(W)$ and $P(W|X, Y)$.

Training a network with dropout (Srivastava et al., 2014) is equivalent to a variational approximation on the network (Gal & Ghahramani, 2016). Furthermore, minimizing the loss function of cross-entropy (CE) (Goodfellow et al., 2016) can have the same effect as minimizing the KL divergence term. Minimizing CE loss in classification problems is equivalent to minimizing mean squared error (MSE) loss in regression problems (Hung et al., 2020; Kline & Berardi, 2005). Therefore, we use the MSE loss function and the root mean squared propagation (RMSProp) optimizer with a learning rate of 0.0002 to train SYMHnet. Table 5 summarizes the hyperparameters and their values used by SYMHnet. We use $\hat{q}(W)$ to represent the optimized weight distribution.

During testing/prediction, SYMHnet uses the MC dropout sampling method (Gal & Ghahramani, 2016) to quantify uncertainty. Specifically, we process the test data $K$ times to generate $K$ MC samples where $K$ is set to 100. We have experimented with different $K$ values. Using a $K$ value of less than 100 does not generate enough samples; the produced uncertainty ranges are too large to be useful. Using a $K$ value of larger than 100 increases computation time, while the model performance remains the same. As a consequence, we set $K$ to 100 to process the test data 100 times. Each time, a set of weights is randomly drawn from $\hat{q}(W)$. We obtain the mean and variance for the $K$ samples. The mean is the anticipated SYM-H value. According to Jiang et al. (2021), we split the variance into aleatoric and epistemic uncertainties.

## 4. Experiments and Results

### 4.1. Performance Metrics

To assess the prediction accuracy of SYMHnet and compare it with related machine learning models, we adopt the following metrics: root mean square error (RMSE), forecast skill score (FSS) and R-squared ($R^2$). These metrics have been used in the forecasting of geomagnetic indices and are recommended in the literature (Camporeale, 2019; Iong et al., 2022; Liemohn et al., 2018). Our experiments were carried out by feeding time series data samples from the training storms in Table 1 (training set) to train a model. We then used the time series data samples from the validation storms in Table 2 (validation set) to validate the model and optimize its hyperparameters. Finally, we used the trained model to predict the SYM-H index values of the time series data samples from the test storms in Table 3 (test set).

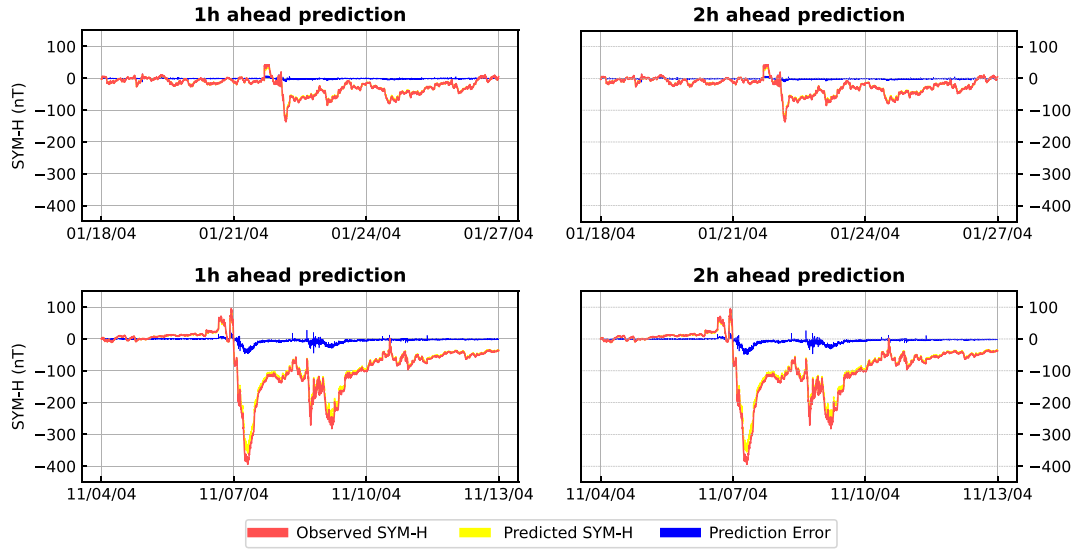


**Figure 3.** Predictions for storm #36 (top) and storm #37 (bottom) made by the SYMHnet model based on 1-min resolution data. The red line represents the observed SYM-H values, the yellow dashed line represents the model's predictions, and the blue line represents the prediction error. Both quiet time and storm time are shown in the figure.

RMSE measures the difference between prediction and ground truth for each test data sample. It is calculated as follows:

$$\mathrm{RMSE} = \sqrt{\frac{1}{n}\sum_{i=1}^{n}\left(y_i - \hat{y}_i\right)^2}, \tag{1}$$

where $n$ is the number of test data samples in a test storm in Table 3, and $\hat{y}_i$ ($y_i$, respectively) represents the predicted SYM-H index value (observed SYM-H index value, respectively) at the time point $i$ in the test storm. The smaller the RMSE, the more accurate the model.

FSS is calculated using the prediction provided by the Burton equation (O'Brien & McPherron, 2000) as a baseline and is defined as follows (Iong et al., 2022; Murphy, 1988):

$$\mathrm{FSS} = 1 - \frac{\frac{1}{n}\sum_{i=1}^{n}\left(y_i - \hat{y}_i\right)^2}{\frac{1}{n}\sum_{i=1}^{n}\left(y_i - y_i^b\right)^2} \tag{2}$$

where $y_i^b$ represents the prediction provided by the Burton equation at the time point $i$ in the test storm. The FSS value between 0 and 1 indicates that the model is better than the baseline, while the negative FSS value indicates that the model is worse than the baseline (Iong et al., 2022).

$R^2$ determines the amount of variance of the observed data explained by the predicted data. It is calculated as follows:

$$R^2 = 1 - \frac{\sum_{i=1}^{n}\left(y_i - \hat{y}_i\right)^2}{\sum_{i=1}^{n}\left(y_i - \bar{y}\right)^2}, \tag{3}$$

where $\bar{y}$ is the mean of the observed SYM-H index values for the test data samples in the test storm. The larger the $R^2$, the more accurate the model.

For each metric, the mean and standard deviation of the metric values for all test storms in the test set (Table 3) are calculated and recorded.

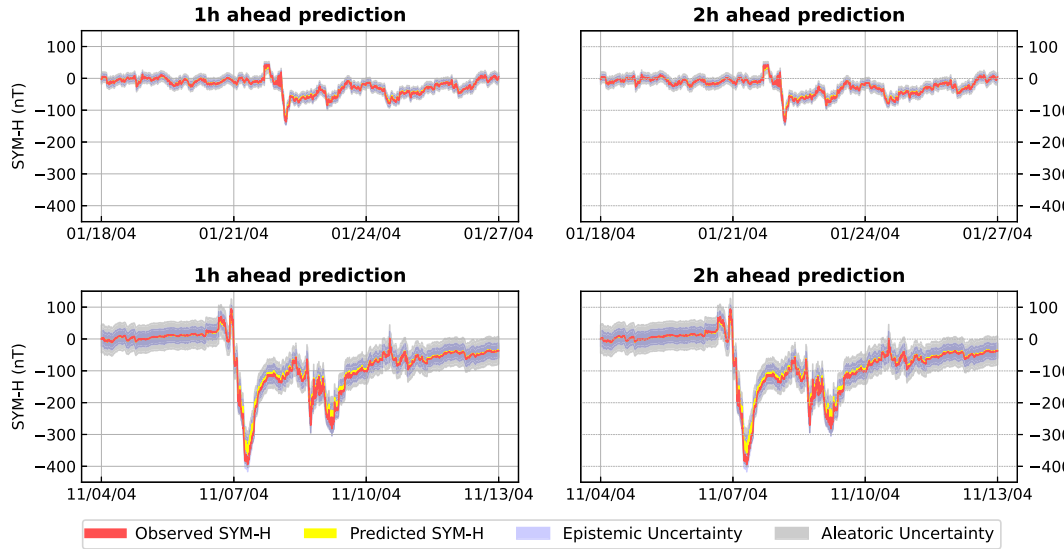


**Figure 4.** Uncertainty quantification results produced by the SYMHnet model in storm #36 (top) and storm #37 (bottom) based on 1-min resolution data. The red line represents the observed SYM-H values, the yellow dashed line represents the model's predictions, the light-blue region shows epistemic uncertainty (model uncertainty), and the light-gray region shows aleatoric uncertainty (data uncertainty). Both quiet time and storm time are shown in the figure.

### 4.2. Results Based on 1-Min Resolution Data

In this section, we present experimental results based on the 1-min resolution data in our database. First, we conducted an ablation study to analyze and assess the components of SYMHnet. Then we performed case studies on a moderately large storm (storm #36 with SYM-H = −137 nT) and a very large storm (storm #37 with SYM-H = −393 nT) in the test set shown in Table 3 where both storms were previously investigated by Iong et al. (2022). It should be noted that the work of Iong et al. (2022) was based on 5-min resolution data. To our knowledge, no previous method used 1-min resolution data to predict the SYM-H index.

#### 4.2.1. Ablation Study With 1-Min Resolution Data

We considered three variants of SYMHnet: SYMHnet-B, SYMHnet-G, and SYMHnet-BG. SYMHnet-B represents the subnetwork of SYMHnet with the BiLSTM component removed. SYMHnet-G represents the subnetwork of SYMHnet with the GNN component removed. SYMHnet-BG represents the subnetwork of SYMHnet with both the BiLSTM and GNN components removed. Thus, SYMHnet-BG simply contains the dense layers in SYMHnet, which amounts to a simple multilayer perceptron network. When conducting the ablation study, we turned off the uncertainty quantification mechanism.

Table 6 presents the average values for RMSE, FSS, and $R^2$ (with standard deviations enclosed in parentheses) obtained by the four models: SYMHnet, SYMHnet-B, SYMHnet-G and SYMHnet-BG, based on the 1-min resolution data in our database. The best metric values are highlighted in boldface. It can be seen from

**Table 7**
*Results of the Ablation Study Based on 5-Min Resolution Data*

| Metric | Hour-ahead | SYMHnet | SYMHnet-B | SYMHnet-G | SYMHnet-BG |
|---|---|---|---|---|---|
| RMSE | 1 | **5.914** (2.169) | 6.324 (2.319) | 8.262 (2.834) | 10.537 (2.958) |
| | 2 | **6.481** (2.201) | 8.646 (2.636) | 13.021 (3.315) | 14.165 (3.194) |
| FSS | 1 | **0.484** (0.195) | 0.407 (0.087) | 0.005 (0.012) | −0.465 (0.023) |
| | 2 | **0.593** (0.096) | 0.302 (0.048) | −0.286 (0.035) | −0.570 (0.042) |
| $R^2$ | 1 | **0.993** (0.003) | 0.912 (0.003) | 0.789 (0.004) | 0.601 (0.005) |
| | 2 | **0.989** (0.003) | 0.905 (0.003) | 0.773 (0.004) | 0.592 (0.005) |

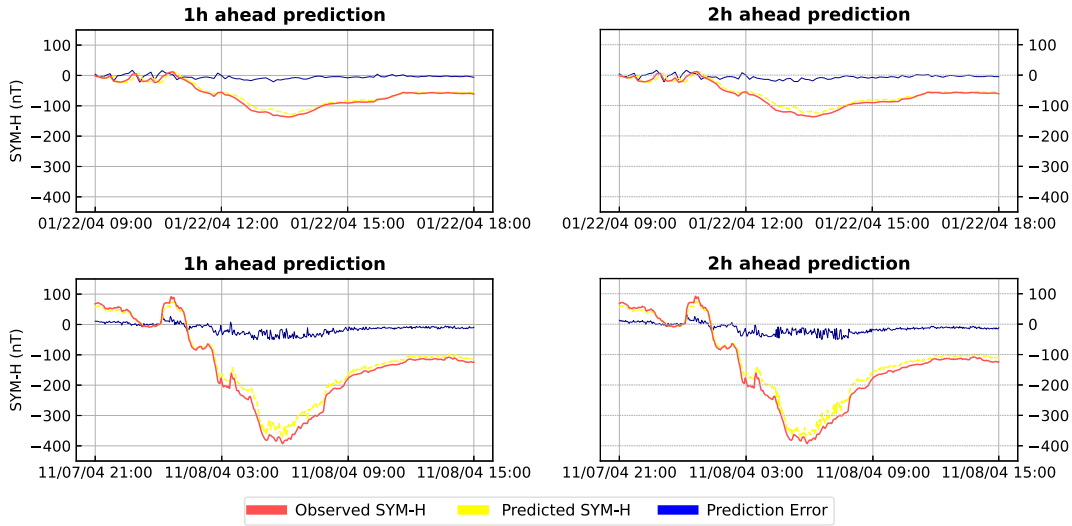


**Figure 5.** Predictions for storm #36 (top) and storm #37 (bottom) made by the SYMHnet model based on 5-min resolution data. The red line represents the observed SYM-H values, the yellow dashed line represents the model's predictions, and the blue line represents the prediction error. Only the peak storm time is shown in the figure.

Table 6 that SYMHnet outperforms its three variants. SYMHnet-B is the second best among the four models, implying that a GNN is effective in solving time series regression problems (Bloemheuvel et al., 2022). SYHMnet-G, which contains a BiLSTM network but no GNN, does not perform well. This finding is consistent with those in Collado-Villaverde et al. (2021), who showed that LSTM performed worse than a combination of LSTM and CNN in SYM-H forecasting. Finally, SYMHnet-BG is the worst among the four models. This happens because SYMHnet-BG loses the advantages offered by GNN and BiLSTM networks.

### 4.2.2. Case Studies With 1-Min Resolution Data

Here we conducted case studies by using SYMHnet to predict the SYM-H index values in storms #36 and #37 given in Table 3 based on the 1-min resolution data in our database. Additional case studies on other storms can be found in Appendix A. The period of storm #36 started on 18 January 2004 and ended on 27 January 2004, with a

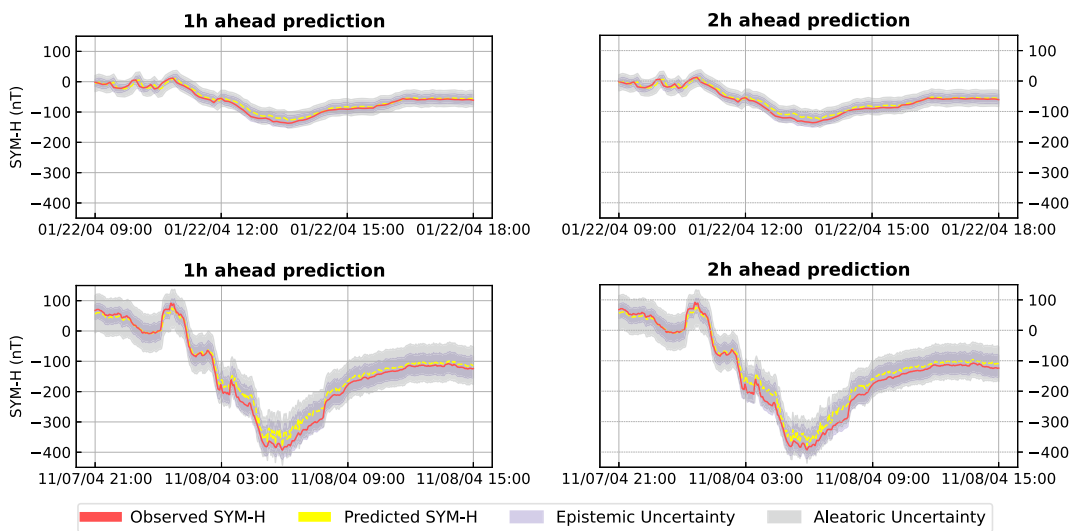


**Figure 6.** Uncertainty quantification results produced by the SYMHnet model in storm #36 (top) and storm #37 (bottom) based on 5-min resolution data. The red line represents the observed SYM-H values, the yellow dashed line represents the model's predictions, the light-blue region shows epistemic uncertainty (model uncertainty), and the light-gray region shows aleatoric uncertainty (data uncertainty). Only the peak storm time is shown in the figure.

**Table 8**
*RMSEs for 1-Hr Ahead Prediction From the Comparative Study Including SYMHnet, LCNN (Collado-Villaverde et al., 2021), GBM (Iong et al., 2022), LSTM and CNN (Siciliano et al., 2021), and Burton Equation (O'Brien & McPherron, 2000)*

| | 1-hr ahead prediction (RMSE) | | | | | |
|---|---|---|---|---|---|---|
| Storm # | SYMHnet | LCNN | GBM | LSTM | CNN | Burton |
| 26 | **3.977** | 6.630 | 5.863 | 6.700 | 7.200 | 6.839 |
| 27 | **7.682** | 8.913 | 7.729 | 8.900 | 10.500 | 7.955 |
| 28 | 4.599 | 5.858 | **4.281** | 5.400 | 5.600 | 5.967 |
| 29 | **5.058** | 6.683 | 5.833 | 7.200 | 7.700 | 6.511 |
| 30 | **2.213** | 5.200 | 4.927 | 5.600 | 6.500 | 4.614 |
| 31 | **7.923** | 8.584 | 8.277 | 10.700 | 9.600 | 8.838 |
| 32 | **3.969** | 7.259 | 6.841 | 8.300 | 8.200 | 9.487 |
| 33 | **11.366** | 13.340 | 14.492 | 16.300 | 19.100 | 16.630 |
| 34 | **5.259** | 10.034 | 10.190 | 11.300 | 12.400 | 10.888 |
| 35 | **5.406** | 7.693 | 7.154 | 8.500 | 8.800 | 7.918 |
| 36 | **5.618** | 9.525 | 8.512 | 8.700 | 10.500 | 9.082 |
| 37 | **10.320** | 15.184 | 14.548 | 17.500 | 17.300 | 15.713 |
| 38 | **3.368** | 4.080 | 3.886 | 4.200 | 4.600 | 4.572 |
| 39 | **5.670** | 6.431 | 5.901 | 5.700 | 6.800 | 6.663 |
| 40 | 5.752 | **4.673** | 4.976 | 5.500 | 5.900 | 5.371 |
| 41 | **5.871** | 7.882 | 7.558 | 9.000 | 9.400 | 8.358 |
| 42 | **3.900** | 5.669 | 5.030 | 5.900 | 6.300 | 5.549 |

*Note.* The best metric values are highlighted in boldface.

minimum SYM-H value of −137 nT and a maximum SYM-H value of 41 nT during the period. The period of storm #37 started on 4 November 2004 and ended on 14 November 2004, with a minimum SYM-H value of −393 nT and a maximum SYM-H value of 92 nT during the period. Figure 3 shows the predictions and measured error of the SYMHnet model in storm #36 and storm #37 respectively. In the figure, each point on a yellow dashed line represents the prediction made at the corresponding time $x$ on the $X$-axis. For 1-hr ahead (2-hr ahead, respectively) predictions, the point/prediction at time $x$ is produced based on the solar wind/IMF parameters at time $x$–1 hr ($x$–2 hr, respectively). There is a lag of 1 hr (for 1-hr ahead predictions) or 2 hr (for 2-hr ahead predictions) as in previous studies (Collado-Villaverde et al., 2021; Iong et al., 2022). It can be seen from Figure 3 that the SYMHnet model works well at both quiet time and storm time. The measured error ranges between −15 and 23 nT for storm #36 and between −50 and 34 nT for storm #37. The more intense the storm, the larger the measured error.

Figure 4 presents uncertainty quantification results produced by SYMHnet in storm #36 and storm #37, respectively, based on the 1-min resolution data in our database. In the figure, the red line represents the observed values of the SYM-H index, and the yellow dashed line represents the predicted values of the SYM-H index. The light-blue region shows the epistemic uncertainty (model uncertainty) and the light-gray region shows the aleatoric uncertainty (data uncertainty) of the predicted outcome. It can be seen in Figure 4 that the yellow dashed line (predicted values) is reasonably close to the red line (observed values), again demonstrating the good performance of SYMHnet. The light-blue region is tinier than the light-gray region, indicating that the model uncertainty is lower than the data uncertainty. This is due to the fact that the uncertainty in the predicted outcome is primarily caused by the noise in the input test data, not by the SYMHnet model.

### 4.3. Results Based on 5-Min Resolution Data

SYMHnet can be easily modified to process 5-min resolution data. As described in Section 3.2, the input data sample at the time point $t$ is composed of the parameter graph $G_t$ and a sequence of $m$ records. The difference is that the cadence of the $m$ records here is 5-min rather than 1-min. Furthermore, the labels of the parameter graphs $G_t$, $G_{t+5}$, $G_{t+10}$ are the SYM-H index values at the time points $t + w$ hour, ($t$ + 5 min) + $w$ hour, ($t$ + 10 min) + $w$ hour, respectively, for $w$-hour ahead predictions where $w$ is 1 or 2.

In the following, we present experimental results based on the 5-min resolution data in our database. As in Section 4.2, we conducted an ablation study, this time using the 5-min resolution data. We then performed case studies on storms #36 and #37. Finally, we compared SYMHnet with related machine learning methods, all of which utilized the 5-min resolution data in our database. Since the related methods cannot quantify uncertainty, we turned off the uncertainty quantification mechanism in SYMHnet while conducting the comparative study.

#### 4.3.1. Ablation Study With 5-Min Resolution Data

Table 7 presents the average values for RMSE, FSS, and $R^2$ (with standard deviations enclosed in parentheses) obtained by the four models: SYMHnet, SYMHnet-B, SYMHnet-G and SYMHnet-BG, based on the 5-min resolution data in our database. The best metric values are highlighted in boldface. It can be seen from Table-7 that SYMHnet is again the best among the four models for the 5-min resolution data, a finding consistent with that in Table 6 for the 1-min resolution data.

**Table 9**
*RMSEs for 2-Hr Ahead Prediction From the Comparative Study Including SYMHnet, LCNN (Collado-Villaverde et al., 2021), GBM (Iong et al., 2022), and Burton Equation (O'Brien & McPherron, 2000)*

| | 2-hr ahead prediction (RMSE) | | | |
|---|---|---|---|---|
| Storm # | SYMHnet | LCNN | GBM | Burton |
| 26 | **4.330** | 8.989 | 8.285 | 10.690 |
| 27 | **8.577** | 13.418 | 11.585 | 12.465 |
| 28 | **4.977** | 5.877 | 5.650 | 8.858 |
| 29 | **5.515** | 9.314 | 8.826 | 9.776 |
| 30 | **2.636** | 7.288 | 7.280 | 6.266 |
| 31 | **9.737** | 12.436 | 12.613 | 13.604 |
| 32 | **4.451** | 8.937 | 9.927 | 13.766 |
| 33 | **13.745** | 18.481 | 24.519 | 25.729 |
| 34 | **5.611** | 13.941 | 13.736 | 14.695 |
| 35 | **5.830** | 9.932 | 9.504 | 10.586 |
| 36 | **5.970** | 12.058 | 12.068 | 13.117 |
| 37 | **10.923** | 21.084 | 22.327 | 24.446 |
| 38 | **3.765** | 5.213 | 5.153 | 6.546 |
| 39 | **6.252** | 6.798 | 7.391 | 10.159 |
| 40 | 6.336 | **5.281** | 5.633 | 6.032 |
| 41 | **6.857** | 11.707 | 12.121 | 12.622 |
| 42 | **4.674** | 8.273 | 7.976 | 8.877 |

*Note.* The best metric values are highlighted in boldface.

**Table 10**
*FSSs for 1-Hr Ahead Prediction From the Comparative Study Including SYMHnet, LCNN (Collado-Villaverde et al., 2021), GBM (Iong et al., 2022), LSTM and CNN (Siciliano et al., 2021)*

| | 1-hr ahead prediction (FSS) | | | | |
|---|---|---|---|---|---|
| Storm # | SYMHnet | LCNN | GBM | LSTM | CNN |
| 26 | **0.418** | 0.031 | 0.143 | 0.020 | −0.053 |
| 27 | **0.034** | −0.120 | 0.028 | −0.119 | −0.320 |
| 28 | 0.229 | −0.028 | **0.249** | 0.095 | 0.062 |
| 29 | **0.223** | −0.026 | 0.104 | −0.106 | −0.183 |
| 30 | **0.520** | −0.127 | −0.068 | −0.214 | −0.409 |
| 31 | **0.104** | 0.029 | 0.063 | −0.211 | −0.086 |
| 32 | **0.582** | 0.235 | 0.279 | 0.125 | 0.136 |
| 33 | **0.317** | 0.198 | 0.129 | 0.020 | −0.149 |
| 34 | **0.517** | 0.078 | 0.064 | −0.038 | −0.139 |
| 35 | **0.317** | 0.028 | 0.096 | −0.074 | −0.111 |
| 36 | **0.381** | −0.049 | 0.063 | 0.042 | −0.156 |
| 37 | **0.343** | 0.034 | 0.074 | −0.114 | −0.101 |
| 38 | **0.263** | 0.108 | 0.150 | 0.081 | −0.006 |
| 39 | **0.149** | 0.035 | 0.114 | 0.160 | −0.021 |
| 40 | −0.071 | **0.130** | 0.074 | −0.024 | −0.098 |
| 41 | **0.298** | 0.057 | 0.096 | −0.077 | −0.125 |
| 42 | **0.297** | −0.022 | 0.094 | −0.063 | −0.135 |

*Note.* The best metric values are highlighted in boldface.

#### 4.3.2. Case Studies With 5-Min Resolution Data

Figure 5 shows the predictions and measured error of SYMHnet in storms #36 and #37, respectively, and Figure 6 presents the uncertainty quantification results produced by SYMHnet in these storms respectively, based on the 5-min resolution data in our database. Unlike Figures 3 and 4, in which both quiet time and storm time are shown, Figures 5 and 6 focus on the peak storm time. In Figure 5, the measured error ranges between −24 and 25 nT for storm #36 and between −52 and 36 nT for storm #37. These results indicate that SYMHnet can properly forecast the SYM-H index even in the most intense storm period.

In Figure 6, the red line represents the observed values of the SYM-H and the yellow dashed line represents the predicted values of the SYM-H. The light-blue area shows the epistemic uncertainty (model uncertainty) and the light-gray area shows the aleatoric uncertainty (data uncertainty) of the predicted outcome. It can be seen from Figure 6 that the red line representing the observed SYM-H values is within the uncertainty interval, indicating SYMHnet's predicted values together with the uncertainty values well cover the observed values. The overall findings here are similar to those from the 1-min resolution data shown in Figure 4.

#### 4.3.3. Comparative Study With 5-Min Resolution Data

Several researchers performed SYM-H forecasting using machine learning and the 5-min resolution data. Collado-Villaverde et al. (2021) combined long short-term memory (LSTM) and a convolutional neural network (CNN), referred to as the LCNN method, to forecast the SYM-H index (1 and 2 hr in advance). Iong et al. (2022) utilized gradient boosting machines, referred to as the GBM method, to forecast the SYM-H index (also 1 and 2 hr in advance). Siciliano et al. (2021) compared LSTM and CNN for the prediction of the SYM-H index (only 1 hr in advance). Although the methods including ours use slightly different data samples, these methods are all developed to predict the SYM-H index values in the same set of storms. The purpose of this comparative study is to compare the prediction results/accuracies of, rather than specific models/data samples in, these methods. This comparison methodology has commonly been used in SYM-H forecasting (Collado-Villaverde et al., 2021; Iong et al., 2022; Siciliano et al., 2021). Since the related methods cannot predict uncertainties, we turned off the uncertainty quantification component in SYMHnet while carrying out the comparative study. The Burton equation (O'Brien & McPherron, 2000), used as the baseline, is also included. The performance metric values of each method for each test storm in the test set (Table 3) are calculated. The best metric values are highlighted in boldface.

Tables 8 and 9 compare the RMSE results of these methods for 1-hr and 2-hr ahead SYM-H predictions, respectively, based on the RMSE values available in the related studies (Collado-Villaverde et al., 2021; Iong et al., 2022; O'Brien & McPherron, 2000; Siciliano et al., 2021). Tables 10 and 11 compare the FSS results of these methods for 1- and 2-hr ahead SYM-H predictions, respectively, based on the FSS values available in the related studies (Collado-Villaverde et al., 2021; Iong et al., 2022; Siciliano et al., 2021). Table 12 compares the $R^2$ results of these methods for 1-hr ahead and 2-hr ahead SYM-H predictions, respectively, on the same test storms. Iong et al. (2022) did not provide $R^2$ results, and hence the GBM method was excluded from Table 12. These tables show that SYMHnet performs better

**Table 11**
*FSSs for 2-Hr Ahead Prediction From the Comparative Study Including SYMHnet, LCNN (Collado-Villaverde et al., 2021), and GBM (Iong et al., 2022)*

| | 2-hr ahead prediction (FSS) | | |
|---|---|---|---|
| Storm # | SYMHnet | LCNN | GBM |
| 26 | **0.595** | 0.159 | 0.225 |
| 27 | **0.312** | −0.076 | 0.071 |
| 28 | **0.438** | 0.337 | 0.362 |
| 29 | **0.436** | 0.047 | 0.097 |
| 30 | **0.579** | −0.163 | −0.162 |
| 31 | **0.284** | 0.086 | 0.073 |
| 32 | **0.677** | 0.351 | 0.279 |
| 33 | **0.466** | 0.282 | 0.047 |
| 34 | **0.618** | 0.051 | 0.065 |
| 35 | **0.449** | 0.062 | 0.102 |
| 36 | **0.545** | 0.081 | 0.080 |
| 37 | **0.553** | 0.138 | 0.087 |
| 38 | **0.425** | 0.204 | 0.213 |
| 39 | **0.385** | 0.331 | 0.272 |
| 40 | −0.050 | **0.125** | 0.066 |
| 41 | **0.457** | 0.072 | 0.040 |
| 42 | **0.473** | 0.068 | 0.101 |

*Note.* The best metric values are highlighted in boldface.

**Table 12**
*$R^2$s for 1- and 2-Hr Ahead Predictions From the Comparative Study Including SYMHnet, LCNN (Collado-Villaverde et al., 2021), LSTM and CNN (Siciliano et al., 2021)*

| | 1-hr ahead prediction ($R^2$) | | | | 2-hr ahead prediction ($R^2$) | |
|---|---|---|---|---|---|---|
| Storm # | SYMHnet | LCNN | LSTM | CNN | SYMHnet | LCNN |
| 26 | **0.956** | 0.870 | 0.890 | 0.870 | **0.948** | 0.766 |
| 27 | **0.952** | 0.939 | 0.940 | 0.920 | **0.940** | 0.862 |
| 28 | **0.957** | 0.936 | 0.950 | 0.950 | **0.949** | 0.936 |
| 29 | **0.955** | 0.922 | 0.930 | 0.920 | **0.946** | 0.848 |
| 30 | **0.991** | 0.946 | 0.950 | 0.930 | **0.987** | 0.894 |
| 31 | **0.976** | 0.971 | 0.960 | 0.970 | **0.963** | 0.939 |
| 32 | **0.986** | 0.953 | 0.950 | 0.950 | **0.982** | 0.929 |
| 33 | **0.979** | 0.965 | 0.960 | 0.950 | **0.969** | 0.932 |
| 34 | **0.945** | 0.798 | 0.750 | 0.700 | **0.938** | 0.612 |
| 35 | **0.954** | 0.907 | 0.900 | 0.890 | **0.947** | 0.845 |
| 36 | **0.949** | 0.864 | 0.890 | 0.840 | **0.943** | 0.782 |
| 37 | **0.993** | 0.966 | 0.960 | 0.960 | **0.992** | 0.934 |
| 38 | **0.961** | 0.939 | 0.940 | 0.930 | **0.951** | 0.900 |
| 39 | **0.964** | 0.932 | 0.960 | 0.940 | **0.943** | 0.924 |
| 40 | 0.948 | **0.966** | 0.950 | 0.950 | 0.937 | **0.957** |
| 41 | **0.984** | 0.969 | 0.960 | 0.960 | **0.978** | 0.931 |
| 42 | **0.985** | 0.968 | 0.970 | 0.960 | **0.978** | 0.932 |

*Note.* The best metric values are highlighted in boldface.

than the related methods for all except two test storms (#28 and/or #40), demonstrating the good performance and feasibility of our tool for SYM-H forecasting.

## 5. Discussion and Conclusion

Geomagnetic activities have a significant impact on Earth, which can cause damages to spacecraft, electrical power grids, and navigation systems. Geospace scientists use geomagnetic indices to measure and quantify the geomagnetic activities. The SYM-H index provides information about the response and behavior of the Earth's magnetosphere during geomagnetic storms. Therefore, a lot of effort has been put into SYM-H forecasting. Previous work mainly focused on 5-min resolution data and skipped 1-min resolution data. The higher temporal resolution of the 1-min resolution data poses a more difficult challenge to forecast due to its highly oscillating character. This oscillating behavior could make the data more noisy to a machine learning model. As a consequence, the model requires more iterations during training with a larger number of neurons in order to learn more features and patterns hidden in the data.

In our study, the SYMHnet model architectures for processing the 1-min resolution data and 5-min resolution data are the same, as shown in Figure-2. The configuration details and hyperparameter values of SYMHnet for processing the 5-min resolution data are shown in Tables 4 and 5. When processing the 1-min resolution data, the model is configured with a larger number of neurons in the dense layers, a higher percentage in the dropout layers, and a larger number of epochs during the training phase. This configuration is designed to combat the highly oscillating behavior of the 1-min resolution data.

Results from our experiments demonstrated the good performance of SYMHnet at both quiet time and storm time. These results were obtained from a database of 42 storms that occurred between 1998 and 2018 during the past two solar cycles (#23 and #24). As done in previous studies (Collado-Villaverde et al., 2021; Iong et al., 2022; Siciliano et al., 2021), 20 storms, listed in Table 1, were used for training, five storms, listed in Table 2, were used for validation, and 17 storms, listed in Table 3, were used for testing. Based on the tables, the 42 storms were distributed to 14 distinct years.

To avoid bias in drawing a conclusion from the above experiments, we conducted an additional experiment using 14-fold cross validation where the data was divided into 14 partitions or folds. Each fold corresponds to 1 year in which at least one storm occurred. The sequential order of the data in each fold was maintained. In each run, one fold was used for testing and the other 13 folds together were used for training. Thus, the training set and test set are disjoint, and the trained model can predict unseen SYM-H values in the test set. There were 14 folds and consequently 14 runs where the average performance metric values over the 14 runs were calculated. The results of the 14-fold cross validation were consistent with those reported in the paper. These results indicate that the SYMHnet tool can be used to predict future SYM-H index values without knowing whether a storm is going to start. When the predicted SYM-H value is less than a threshold (e.g., −30 nT), the tool detects the occurrence of a storm. Thus, we conclude that the proposed SYMHnet is a viable machine learning method for short-term, 1 or 2-hr ahead forecasts of the SYM-H index for both 1- and 5-min resolution data.

## Appendix A: Additional Case Studies With 1-Min Resolution Data

Figure A1 shows the predictions and measured error of SYMHnet in storms #28, #31, #33, #40, and #42, respectively, and Figure A2 presents the uncertainty quantification results produced by SYMHnet in these storms, respectively, based on the 1-min resolution data in our database. The period of storm #28 started on 9 January 1999 and ended on 18 January 1999, with a minimum SYM-H value of −111 nT and a maximum SYM-H value of 9 nT. The period of storm #31 started on 2 April 2000 and ended on 12 April 2000, with a minimum SYM-H value

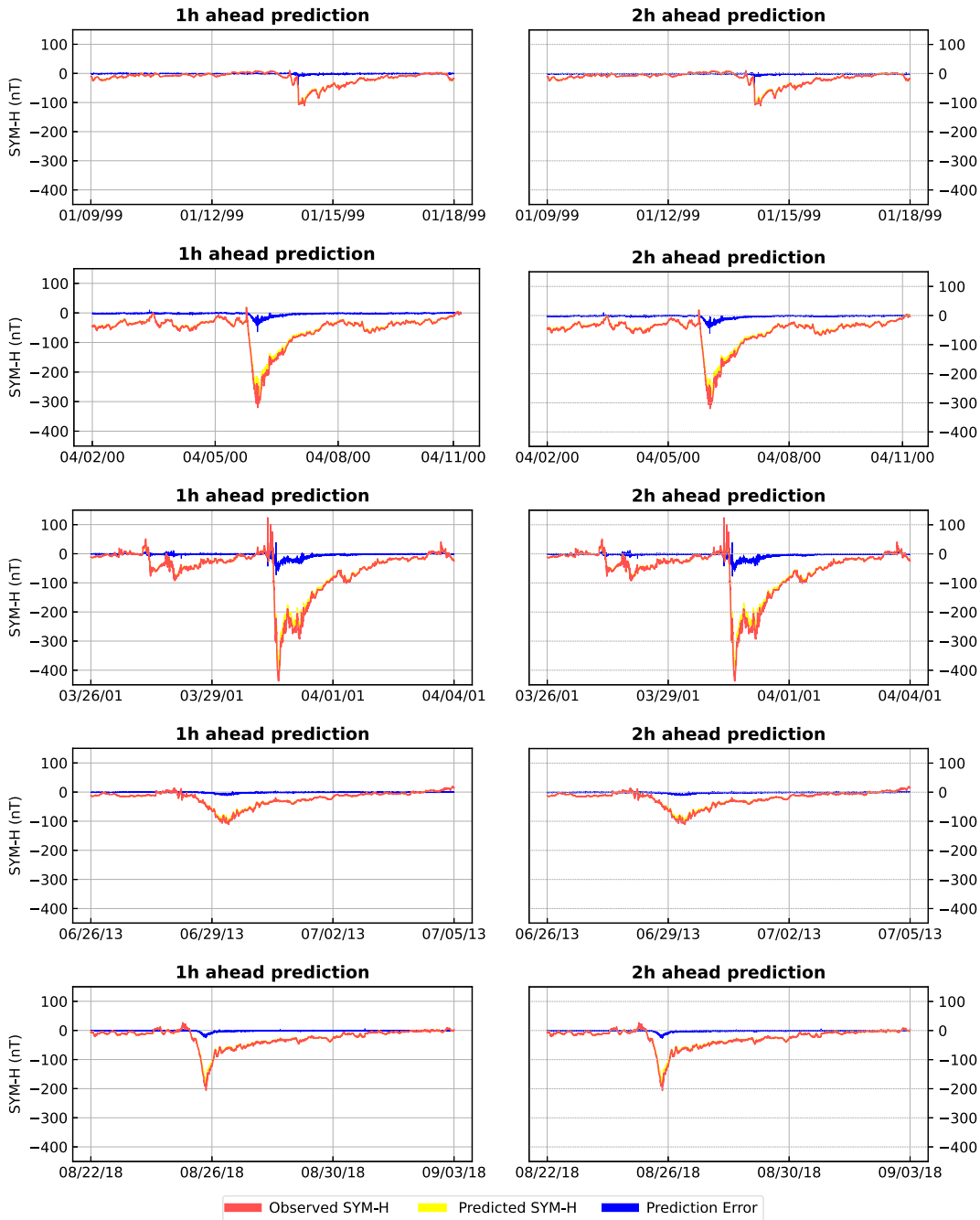


**Figure A1.** Predictions for storms (from top to bottom) #28 in January 1999, #31 in April 2000, #33 in March 2001, #40 in June 2013, and #42 in August 2018, made by the SYMHnet model based on 1-min resolution data. The red line represents the observed SYM-H values, the yellow dashed line represents the model's predictions, and the blue line represents the prediction error. Both quiet time and storm time are shown in the figure.

10.1029/2023SW003824

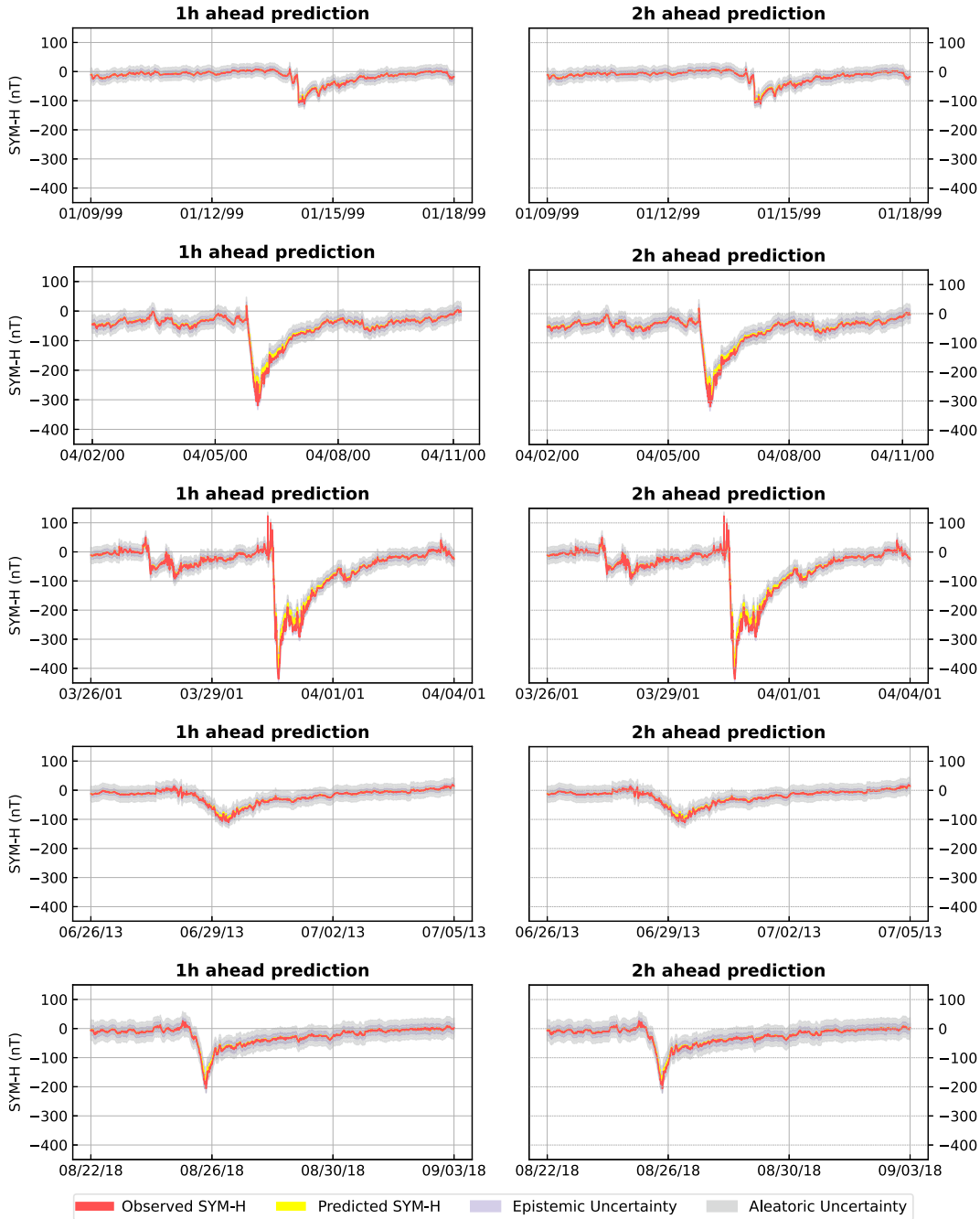


**Figure A2.** Uncertainty quantification results produced by the SYMHnet model in storms (from top to bottom) #28 in January 1999, #31 in April 2000, #33 in March 2001, #40 in June 2013, and #42 in August 2018, based on 1-min resolution data. The red line represents the observed SYM-H values, the yellow dashed line represents the model's predictions, the light-blue region shows epistemic uncertainty (model uncertainty), and the light-gray region shows aleatoric uncertainty (data uncertainty). Both quiet time and storm time are shown in the figure.

of −315 nT and a maximum SYM-H value of 16 nT. The period of storm #33 stared on 26 March 2001 and ended on 4 April 2001, with a minimum SYM-H value of −434 nT and a maximum SYM-H value of 109 nT. The period of storm #40 started on 26 June 2013 and ended on 4 July 2013, with a minimum SYM-H value of −110 nT and a maximum SYM-H value of 19 nT. The period of storm #42 started on 22 August 2018 and ended on 3 September 2018, with a minimum SYM-H value of −205 nT and a maximum SYM-H value of 26 nT. In Figure A1, the measured error ranges between −46 and 7 nT for storm #28, between −58 and 2 nT for storm #31, between −69

and 32 nT for storm #33, between −12 and 4 nT for storm #40, and between −26 and 7 nT for storm #42. Generally, the more intense the storm, the larger the measured error. In Figure A2, we see that SYMHnet's predicted values together with the uncertainty values well cover the observed values, a finding consistent with that in Figure 4.

## Data Availability Statement

- The solar wind, IMF and derived parameters along with the SYM-H index data used in our study are publicly available from NASA's Space Physics Data Facility at http://omniweb.gsfc.nasa.gov/ow.html.
- Details of SYMHnet can be found at https://doi.org/10.5281/zenodo.10602518.

**Acknowledgments**
We appreciate the editor and anonymous referees for constructive comments and suggestions. We acknowledge the use of NASA/GSFC's Space Physics Data Facility's OMNIWeb and CDAWeb services, and OMNI data. This work was supported in part by U.S. NSF Grants AGS-1927578, AGS-1954737, AGS-2149748, AGS-2228996, AGS-2300341 and OAC-2320147. Huseyin Cavus was supported by the Fulbright Visiting Scholar Program of the Turkish Fulbright Commission.

## References

Abduallah, Y., Jordanova, V. K., Liu, H., Li, Q., Wang, J. T. L., & Wang, H. (2022). Predicting solar energetic particles using SDO/HMI vector magnetic data products and a bidirectional LSTM network. *The Astrophysical Journal - Supplement Series*, *260*(1), 16. https://doi.org/10.3847/1538-4365/ac5f56

Abduallah, Y., Wang, J. T. L., Nie, Y., Liu, C., & Wang, H. (2021). DeepSun: Machine-learning-as-a-service for solar flare prediction. *Research in Astronomy and Astrophysics*, *21*(7), 160. https://doi.org/10.1088/1674-4527/21/7/160

Alobaid, K. A., Abduallah, Y., Wang, J. T. L., Wang, H., Jiang, H., Xu, Y., et al. (2022). Predicting CME arrival time through data integration and ensemble learning. *Frontiers in Astronomy and Space Sciences*, *9*, 1013345. https://doi.org/10.3389/fspas.2022.1013345

Amata, E., Pallocchia, G., Consolini, G., Marcucci, M. F., & Bertello, I. (2008). Comparison between three algorithms for Dst predictions over the 2003–2005 period. *Journal of Atmospheric and Solar-Terrestrial Physics*, *70*(2–4), 496–502. https://doi.org/10.1016/j.jastp.2007.08.041

Ayala Solares, J. R., Wei, H.-L., Boynton, R. J., Walker, S. N., & Billings, S. A. (2016). Modeling and prediction of global magnetic disturbance in near-Earth space: A case study for Kp index using NARX models. *Space Weather*, *14*(10), 899–916. https://doi.org/10.1002/2016SW001463

Bala, R., & Reiff, P. (2012). Improvements in short-term forecasting of geomagnetic activity. *Space Weather*, *10*(6). https://doi.org/10.1029/2012SW000779

Bhaskar, A., & Vichare, G. (2019). Forecasting of SYMH and ASYH indices for geomagnetic storms of solar cycle 24 including St. Patrick's day, 2015 storm using NARX neural network. *Journal of Space Weather and Space Climate*, *9*(A12), A12. https://doi.org/10.1051/swsc/2019007

Bloemheuvel, S., van den Hoogen, J., Jozinović, D., Michelini, A., & Atzmueller, M. (2022). Graph neural networks for multivariate time series regression with application to seismic data. *International Journal of Data Science and Analytics*, *16*(3), 317–332. https://doi.org/10.1007/s41060-022-00349-6

Burton, R. K., McPherron, R. L., & Russell, C. T. (1975). An empirical relationship between interplanetary conditions and Dst. *Journal of Geophysical Research*, *80*(31), 4204–4214. https://doi.org/10.1029/JA080i031p04204

Cai, L., Ma, S. Y., & Zhou, Y. L. (2010). Prediction of SYM-H index during large storms by NARX neural network from IMF and solar wind data. *Annales Geophysicae*, *28*(2), 381–393. https://doi.org/10.5194/angeo-28-381-2010

Camporeale, E. (2019). The challenge of machine learning in space weather: Nowcasting and forecasting. *Space Weather*, *17*(8), 1166–1207. https://doi.org/10.1029/2018SW002061

Carter, B. A., Yizengaw, E., Pradipta, R., Weygand, J. M., Piersanti, M., Pulkkinen, A., et al. (2016). Geomagnetically induced currents around the world during the 17 March 2015 storm. *Journal of Geophysical Research: Space Physics*, *121*(10), 10496–10507. https://doi.org/10.1002/2016JA023344

Chandorkar, M., Camporeale, E., & Wing, S. (2017). Probabilistic forecasting of the disturbance storm time index: An autoregressive Gaussian process approach. *Space Weather*, *15*(8), 1004–1019. https://doi.org/10.1002/2017SW001627

Chen, Y., Manchester, W. B., Hero, A. O., Toth, G., DuFumier, B., Zhou, T., et al. (2019). Identifying solar flare precursors using time series of SDO/HMI images and SHARP parameters. *Space Weather*, *17*(10), 1404–1426. https://doi.org/10.1029/2019SW002214

Collado-Villaverde, A., Muñoz, P., & Cid, C. (2021). Deep neural networks with convolutional and LSTM layers for SYM-H and ASY-H forecasting. *Space Weather*, *19*(6), e02748. https://doi.org/10.1029/2021SW002748

Consolini, G., & Chang, T. S. (2001). Magnetic field topology and criticality in geotail dynamics: Relevance to substorm phenomena. *Space Science Reviews*, *95*(1/2), 309–321. https://doi.org/10.1023/A:1005252807049

Denker, J. S., & LeCun, Y. (1990). Transforming neural-net output levels to probability distributions. In *Proceedings of the 3rd International Conference on Neural Information Processing Systems* (pp. 853–859).

Denton, M. H., Henderson, M. G., Jordanova, V. K., Thomsen, M. F., Borovsky, J. E., Woodroffe, J., et al. (2016). An improved empirical model of electron and ion fluxes at geosynchronous orbit based on upstream solar wind conditions. *Space Weather*, *14*(7), 511–523. https://doi.org/10.1002/2016SW001409

Gal, Y., & Ghahramani, Z. (2016). Dropout as a Bayesian approximation: Representing model uncertainty in deep learning. In *Proceedings of the 33rd International Conference on Machine Learning* (pp. 1050–1059). https://doi.org/10.5555/3045390.3045502

Gaunt, C. T., & Coetzee, G. (2007). Transformer failures in regions incorrectly considered to have low GIC-risk. In *2007 IEEE Lausanne Power Tech* (pp. 807–812). https://doi.org/10.1109/PCT.2007.4538419

Gleisner, H., Lundstedt, H., & Wintoft, P. (1996). Predicting geomagnetic storms from solar-wind data using time-delay neural networks. *Annales Geophysicae*, *14*(7), 679–686. https://doi.org/10.1007/s005850050332

Goodfellow, I. J., Bengio, Y., & Courville, A. C. (2016). *Deep learning*. MIT Press.

Graves, A. (2011). Practical variational inference for neural networks. In J. Shawe-Taylor, R. Zemel, P. Bartlett, F. Pereira, & K. Q. Weinberger (Eds.), *Advances in neural information processing systems* (Vol. 24). Curran Associates, Inc.

Gruet, M. A., Chandorkar, M., Sicard, A., & Camporeale, E. (2018). Multiple-hour-ahead forecast of the Dst index using a combination of long short-term memory neural network and Gaussian process. *Space Weather*, *16*(11), 1882–1896. https://doi.org/10.1029/2018SW001898

Hochreiter, S., & Schmidhuber, J. (1997). Long short-term memory. *Neural Computation*, *9*(8), 1735–1780. https://doi.org/10.1162/neco.1997.9.8.1735

Huang, X., Wang, H., Xu, L., Liu, J., Li, R., & Dai, X. (2018). Deep learning based solar flare forecasting model. I. Results for line-of-sight magnetograms. *The Astrophysical Journal*, *856*(1), 7. https://doi.org/10.3847/1538-4357/aaae00

Hung, C.-C., Chen, Y.-J., Guo, S. J., & Hsu, F.-C. (2020). Predicting the price movement from candlestick charts: A CNN-based approach. *International Journal of Ad Hoc and Ubiquitous Computing*, *34*(2), 111–120. https://doi.org/10.1504/IJAHUC.2020.107821

Iong, D., Chen, Y., Toth, G., Zou, S., Pulkkinen, T., Ren, J., et al. (2022). New findings from explainable SYM-H forecasting using gradient boosting machines. *Space Weather*, *20*(8), e2021SW002928. https://doi.org/10.1029/2021SW002928

Jiang, H., Jing, J., Wang, J., Liu, C., Li, Q., Xu, Y., & Wang, H. (2021). Tracing H$\alpha$ fibrils through Bayesian deep learning. *The Astrophysical Journal - Supplement Series*, *256*(1), 20. https://doi.org/10.3847/1538-4365/ac14b7

Jordanova, V. K., Ilie, R., & Chen, M. W. (2020). *Ring current investigations: The quest for space weather prediction*. Elsevier. https://doi.org/10.1016/C2017-0-03448-1

Kendall, A., & Gal, Y. (2017). What uncertainties do we need in Bayesian deep learning for computer vision? In I. Guyon, U. V. Luxburg, S. Bengio, H. Wallach, R. Fergus, S. Vishwanathan, & R. Garnett (Eds.), *Advances in neural information processing systems* (Vol. 30). Curran Associates, Inc.

King, J. H., & Papitashvili, N. E. (2005). Solar wind spatial scales in and comparisons of hourly wind and ACE plasma and magnetic field data. *Journal of Geophysical Research*, *110*(A2). https://doi.org/10.1029/2004JA010649

Klimas, A. J., Vassiliadis, D., Baker, D. N., & Roberts, D. A. (1996). The organized nonlinear dynamics of the magnetosphere. *Journal of Geophysical Research*, *101*(A6), 13089–13113. https://doi.org/10.1029/96JA00563

Kline, M., & Berardi, L. (2005). Revisiting squared-error and cross-entropy functions for training neural network classifiers. *Neural Computing & Applications*, *14*(4), 310–318. https://doi.org/10.1007/s00521-005-0467-y

Laurenza, M., Cliver, E. W., Hewitt, J., Storini, M., Ling, A. G., Balch, C. C., & Kaiser, M. L. (2009). A technique for short-term warning of solar energetic particle events based on flare location, flare size, and evidence of particle escape. *Space Weather*, *7*(4), S04008. https://doi.org/10.1029/2007SW000379

Lavasa, E., Giannopoulos, G., Papaioannou, A., Anastasiadis, A., Daglis, I. A., Aran, A., et al. (2021). Assessing the predictability of solar energetic particles with the use of machine learning techniques. *Solar Physics*, *296*(7), 107. https://doi.org/10.1007/s11207-021-01837-x

Lazzús, J. A., Vega, P., Rojas, P., & Salfate, I. (2017). Forecasting the Dst index using a swarm-optimized neural network. *Space Weather*, *15*(8), 1068–1089. https://doi.org/10.1002/2017SW001608

Liemohn, M. W., McCollough, J. P., Jordanova, V. K., Ngwira, C. M., Morley, S. K., Cid, C., et al. (2018). Model evaluation guidelines for geomagnetic index predictions. *Space Weather*, *16*(12), 2079–2102. https://doi.org/10.1029/2018SW002067

Liu, H., Liu, C., Wang, J. T. L., & Wang, H. (2019). Predicting solar flares using a long short-term memory network. *The Astrophysical Journal*, *877*(2), 121. https://doi.org/10.3847/1538-4357/ab1b3c

Liu, H., Liu, C., Wang, J. T. L., & Wang, H. (2020). Predicting coronal mass ejections using SDO/HMI vector magnetic data products and recurrent neural networks. *The Astrophysical Journal*, *890*(1), 12. https://doi.org/10.3847/1538-4357/ab6850

Lu, J., Peng, Y., Wang, M., Gu, S., & Zhao, M. (2016). Support vector machine combined with distance correlation learning for Dst forecasting during intense geomagnetic storms. *Planetary and Space Science*, *120*, 48–55. https://doi.org/10.1016/j.pss.2015.11.004

Mayaud, P. N. (1980). What is a geomagnetic index? In *Derivation, meaning, and use of geomagnetic indices* (pp. 2–4). American Geophysical Union (AGU). https://doi.org/10.1002/9781118663837.ch2

Moldwin, M. B., & Tsu, J. S. (2016). Stormtime equatorial electrojet ground-induced currents. In *Ionospheric space weather* (pp. 33–40). American Geophysical Union (AGU). https://doi.org/10.1002/9781118929216.ch3

Murphy, A. H. (1988). Skill scores based on the mean square error and their relationships to the correlation coefficient. *Monthly Weather Review*, *116*(12), 2417–2424. https://doi.org/10.1175/1520-0493(1988)116<2417:SSBOTM>2.0.CO;2

Newell, P. T., Sotirelis, T., Liou, K., Meng, C.-I., & Rich, F. J. (2007). A nearly universal solar wind-magnetosphere coupling function inferred from 10 magnetospheric state variables. *Journal of Geophysical Research*, *112*(A1). https://doi.org/10.1029/2006JA012015

Núñez, M. (2011). Predicting solar energetic proton events (E > 10 MeV). *Space Weather*, *9*(7). https://doi.org/10.1029/2010SW000640

Nuraeni, F., Ruhimat, M., Aris, M. A., Ratnasari, E. A., & Purnomo, C. (2022). Development of 24 hours Dst index prediction from solar wind data and IMF Bz using NARX. *Journal of Physics: Conference Series*, *2214*(1), 012024. https://doi.org/10.1088/1742-6596/2214/1/012024

O'Brien, T. P., & McPherron, R. L. (2000). An empirical phase space analysis of ring current dynamics: Solar wind control of injection and decay. *Journal of Geophysical Research*, *105*(A4), 7707–7719. https://doi.org/10.1029/1998JA000437

Pallocchia, G., Amata, E., Consolini, G., Marcucci, M. F., & Bertello, I. (2006). Geomagnetic Dst index forecast based on IMF data only. *Annales Geophysicae*, *24*(3), 989–999. https://doi.org/10.5194/angeo-24-989-2006

Panagopoulos, G., Nikolentzos, G., & Vazirgiannis, M. (2021). Transfer graph neural networks for pandemic forecasting. In *Proceedings of the Thirty-Fifth AAAI Conference on Artificial Intelligence* (pp. 4838–4845). https://doi.org/10.1609/aaai.v35i6.16616

Rangarajan, G. K. (1989). Indices of geomagnetic activity. *Geomatik*, *3*, 323–384.

Rastätter, L., Kuznetsova, M. M., Glocer, A., Welling, D., Meng, X., Raeder, J., et al. (2013). Geospace environment modeling 2008-2009 challenge: Dst index. *Space Weather*, *11*(4), 187–205. https://doi.org/10.1002/swe.20036

Siami-Namini, S., Tavakoli, N., & Namin, A. S. (2019). The performance of LSTM and BiLSTM in forecasting time series. In *IEEE International Conference on Big Data* (pp. 3285–3292). https://doi.org/10.1109/BigData47090.2019.9005997

Siciliano, F., Consolini, G., Tozzi, R., Gentili, M., Giannattasio, F., & De Michelis, P. (2021). Forecasting SYM-H index: A comparison between long short-term memory and convolutional neural networks. *Space Weather*, *19*(2), e2020SW002589. https://doi.org/10.1029/2020SW002589

Srivastava, N., Hinton, G., Krizhevsky, A., Sutskever, I., & Salakhutdinov, R. (2014). Dropout: A simple way to prevent neural networks from overfitting. *Journal of Machine Learning Research*, *15*(56), 1929–1958. Retrieved from http://jmlr.org/papers/v15/srivastava14a.html

Stumpo, M., Benella, S., Laurenza, M., Alberti, T., Consolini, G., & Marcucci, M. F. (2021). Open issues in statistical forecasting of solar proton events: A machine learning perspective. *Space Weather*, *19*(10), e2021SW002794. https://doi.org/10.1029/2021SW002794

Temerin, M., & Li, X. (2002). A new model for the prediction of Dst on the basis of the solar wind. *Journal of Geophysical Research*, *107*(A12), SMP31-1–SMP31-8. https://doi.org/10.1029/2001JA007532

Tozzi, R., De Michelis, P., Coco, I., & Giannattasio, F. (2019). A preliminary risk assessment of geomagnetically induced currents over the Italian territory. *Space Weather*, *17*(1), 46–58. https://doi.org/10.1029/2018SW002065

Vichare, G., Thomas, N., Shiokawa, K., Bhaskar, A., & Sinha, A. K. (2019). Spatial gradients in geomagnetic storm time currents observed by Swarm multispacecraft mission. *Journal of Geophysical Research: Space Physics*, *124*(2), 982–995. https://doi.org/10.1029/2018JA025692

Viljanen, A., Pirjola, R., Prácser, E., Katkalov, J., & Wik, M. (2014). Geomagnetically induced currents in Europe - Modelled occurrence in a continent-wide power grid. *Journal of Space Weather and Space Climate*, *4*(A09), A09. https://doi.org/10.1051/swsc/2014006

Volodina, V., & Challenor, P. (2021). The importance of uncertainty quantification in model reproducibility. *Philosophical Transactions of the Royal Society A: Mathematical, Physical and Engineering Sciences*, *379*(2197), 20200071. https://doi.org/10.1098/rsta.2020.0071

Wang, C. B., Chao, J. K., & Lin, C.-H. (2003). Influence of the solar wind dynamic pressure on the decay and injection of the ring current. *Journal of Geophysical Research*, *108*(A9). https://doi.org/10.1029/2003JA009851

Wanliss, J. A., & Showalter, K. M. (2006). High-resolution global storm index: Dst versus SYM-H. *Journal of Geophysical Research*, *111*(A2), A02202. https://doi.org/10.1029/2005JA011034

Woodroffe, J. R., Morley, S. K., Jordanova, V. K., Henderson, M. G., Cowee, M. M., & Gjerloev, J. G. (2016). The latitudinal variation of geoelectromagnetic disturbances during large (Dst ≤ -100 nT) geomagnetic storms. *Space Weather*, *14*(9), 668–681. https://doi.org/10.1002/2016SW001376

Xu, W., Zhu, Y., Zhu, L., Lu, J., Wei, G., Wang, M., & Peng, Y. (2023). A class of Bayesian machine learning model for forecasting Dst during intense geomagnetic storms. *Advances in Space Research*, *72*(9), 3882–3889. https://doi.org/10.1016/j.asr.2023.07.009

Yurchyshyn, V., Wang, H., & Abramenko, V. (2004). Correlation between speeds of coronal mass ejections and the intensity of geomagnetic storms. *Space Weather*, *2*(2), S02001. https://doi.org/10.1029/2003SW000020